rotations about the C_3 axis of the molecule, or more precisely, concerted rotations of the ligands about the C_2 axes.

Acknowledgment. We wish to thank the National Science Foundation for financial assistance through its Departmental Instrument Program (Grant GP-28235) and Mr. D. J. Olszanski for the preparation of $Sc(trop)_3$.

Registry No. $Sc(C_7H_5O_2)_3$, 15388-96-2.

Supplementary Material Available. A listing of structure factor amplitudes will appear following these pages in the microfilm edition of this volume of the journal. Photocopies of the supplementary material from this paper only or microfiche (105 × 148 mm, 20 × reduction, negatives) containing all of the supplementary material for the papers in this issue may be obtained from the Journals Department, American Chemical Society, 1155 16th St., N.W., Washington, D. C. 20036. Remit check or money order for $3.00 for photocopy or $2.00 for microfiche, referring to code number INORG-74-158.

Contribution from the Department of Chemistry, University of Kansas, Lawrence, Kansas 66044

Oxidation of Substituted Borane Anions to Coupled Polyhedral Ions[1]

A. P. SCHMITT and R. L. MIDDAUGH*

Received March 23, 1973

Electrochemical oxidations of both apical and equatorial isomers of $B_{10}H_9I^{2-}$ and $B_{10}H_9L^-$ (L = NH_3, $N(CH_3)_3$, $S(CH_3)_2$) ions have been studied in acetonitrile. Their behavior is analogous to that of the unsubstituted $B_{10}H_{10}^{2-}$ ion described in eq 1-3. The chemistry of the resulting $B_{20}H_{17}L_2^-$ and $B_{20}H_{16}L_2^{2-}$ ions and $B_{20}H_{16}L_2$ compounds parallels that of the unsubstituted $B_{20}H_{19}^{3-}$, $B_{20}H_{18}^{4-}$, and $B_{20}H_{18}^{2-}$ ions. The rates of reaction 2 for equatorial isomers show an increase with electron withdrawal as indicated by substituent σ_m values, which indicates that equatorial substituents have a primarily inductive effect on this reaction. Apical substituents have a more pronounced effect on the rates of reaction 2; an inversion of substituent effect is indicative of a change in the rate-limiting step under conditions of strong electron withdrawal.

$$B_{10}H_{10}^{2-} \rightleftarrows B_{10}H_{10}^{\cdot -} + e^- \quad (1)$$

$$2B_{10}H_{10}^{\cdot -} \rightarrow B_{20}H_{19}^{3-} + H^+ \quad (2)$$

$$B_{20}H_{19}^{3-} \rightarrow B_{20}H_{18}^{2-} + H^+ + 2e^- \quad (3)$$

Introduction

Aqueous chemical oxidation of $B_{10}H_{10}^{2-}$ ion provided access to the interesting isomerism and redox chemistry of the $B_{20}H_{19}^{3-}$, $B_{20}H_{18}^{4-}$, and $B_{20}H_{18}^{2-}$ ions summarized in Scheme I. For the isomeric $B_{20}H_{18}^{4-}$ ions, the prefixes denote

Scheme I

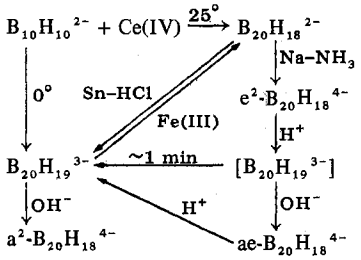

the linkages between B_{10} polyhedra shown in Figure 1, with a^2 indicating a B-B bond between apex boron atoms of the two B_{10} units, etc. The structure of the stable isomer of $B_{20}H_{19}^{3-}$ is apparently similar to that of ae-$B_{20}H_{18}^{4-}$, but with the B-B bond between B_{10} units protonated to form a BHB three-center bridge bond.[2] The structure of the unstable isomer of $B_{20}H_{19}^{3-}$ enclosed in brackets in Scheme I is not known, as it rapidly isomerizes in solution to the stable form.[2] Electrochemical oxidation of $B_{10}H_{10}^{2-}$ ion in acetonitrile parallels the aqueous chemical oxidation and is summarized by eq 1-3.[3]

$$B_{10}H_{10}^{2-} \rightleftarrows B_{10}H_{10}^{\cdot -} + e^- \quad (1)$$

$$2B_{10}H_{10}^{\cdot -} \rightarrow B_{20}H_{19}^{3-} + H^+ \quad (2)$$

$$B_{20}H_{19}^{3-} \rightleftarrows B_{20}H_{18}^{2-} + H^+ + 2e^- \quad (3)$$

Relatively little is known about the reactions in Scheme I for substituted derivatives of $B_{10}H_{10}^{2-}$. The $B_{20}H_{18}^{2-}$ ion is subject to attack by hydroxide and methoxide ions, which leads to the chemistry of the B_{20} derivative ions $B_{20}H_{18}OR^{3-}$, $B_{20}H_{17}OR^{4-}$, and $B_{20}H_{17}OR^{2-}$.[4] Aqueous chemical oxidations of $B_{10}H_9L^-$ ions (L = $(CH_3)_2S$, tetramethylene sulfone, C_6H_5I, or $C_6H_5NO_2$) yield $B_{20}H_{16}L_2$ compounds which are derivatives of the $B_{20}H_{18}^{2-}$ ion (difference in overall charge can be viewed as resulting from substitution of a neutral Lewis base L for hydride ion as a "ligand" to boron). These $B_{20}H_{16}L_2$ compounds undergo the same reaction with base as does the $B_{20}H_{18}^{2-}$ ion.[5]

Electrochemical techniques can often be used to measure relatively rapid chemical reactions that follow electron transfers, such as reaction 2, and often provide clean and well-controlled conditions under which to carry out redox reactions on a preparative scale. We have examined the electrochemical oxidation of both apex and equatorial isomers of some derivatives of $B_{10}H_{10}^{2-}$ to determine their behavior in the context of Scheme I and the effect of substituents on reactions 1-3.

(1) (a) Acknowledgment is made to the donors of the Petroleum Research Fund, administered by the American Chemical Society, and to the University of Kansas General Research Fund, for partial support of this research. (b) Taken in part from the Ph.D. thesis of A. P. Schmitt, University of Kansas, 1970.

(2) M. F. Hawthorne, R. L. Pilling, and P. F. Stokely, *J. Amer. Chem. Soc.*, 87, 1893 (1965).

(3) R. L. Middaugh and F. Farha, Jr., *J. Amer. Chem. Soc.*, 88, 4147 (1966).

(4) M. F. Hawthorne, R. L. Pilling, and P. M. Garrett, *J. Amer. Chem. Soc.*, 87, 4740 (1965).

(5) B. L. Chamberland and E. L. Muetterties, *Inorg. Chem.*, 3, 1450 (1964).

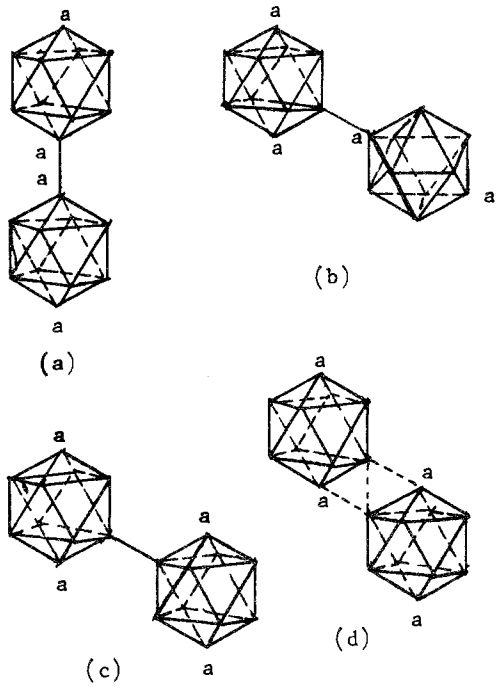

Figure 1. Structures of B_{20} ions. Apical positions (1 and 10 in the official numbering system) of the B_{10} units are labeled a. Equatorial positions (2-9) are unlabeled: (a) a^2 isomer of $B_{20}H_{18}^{4-}$; (b) ae isomer of $B_{20}H_{18}^{4-}$; (c) e^2 isomer of $B_{20}H_{18}^{4-}$; (d) $B_{20}H_{18}^{2-}$.

Results

Cyclic Voltammetry of B_{10} Species. A cyclic voltammogram for $1\text{-}B_{10}H_9S(CH_3)_2^-$, representative of all the compounds in this study, is shown in Figure 2. Current peaks A and B are the oxidations to be discussed; peak C was not investigated. Peak D, the reduction of H^+, appears only after peaks A and/or B have been traversed. Current peak E appears only after peak B has been traversed, and does not appear if the scan is reversed after peak A but before peak B.

For the first anodic process (peak A), the potential at half the peak current, $E_{p/2}$, relative to a saturated aqueous calomel electrode, for each compound was essentially independent of concentration and scan rate and was used to characterize the compounds. The results are listed in Table I.

Preparation and Cyclic Voltammetry of $B_{20}H_{17}L_2^-$ Ions. Solutions of the $B_{10}H_9L^-$ ions in acetonitrile were electrolyzed at potentials about equal to the potential of peak A in the cyclic voltammograms until about 1.0 equiv of current/mol of $B_{10}H_9L^-$ had passed and the current had dropped to a few per cent of the initial current. Products were isolated as tetrapropylammonium salts. Nmr data are given in Table II.

Voltammograms of the $B_{20}H_{17}L_2^-$ ions were virtually identical with those of the corresponding $B_{10}H_9L^-$ ions, except that peak A was absent. Values of $E_{p/2}$ *vs.* sce for the oxidation of $B_{20}H_{17}L_2^-$ ions, corresponding to peak B in Figure 2, were +1.02 V (L = $1\text{-}N(CH_3)_3$), +1.06 V ($2\text{-}N(CH_3)_3$), + 1.21 V ($1\text{-}S(CH_3)_2$), + 1.20 V ($2\text{-}S(CH_3)_2$).

Preparation and Cyclic Voltammetry of $B_{20}H_{16}L_2$ Compounds. Solutions of the $B_{10}H_9L^-$ ions in acetonitrile were electrolyzed at potentials corresponding to peak B of Figure 2 until 2.0 equiv of current had passed and the current had dropped to a few per cent of the original current. The compounds were recrystallized from acetonitrile–ethanol mixtures. Nmr spectral data are given in Table III.

A cyclic voltammogram of $B_{20}H_{16}L_2$ with L = $1\text{-}S(CH_3)_2$, representative of the $B_{20}H_{16}L_2$ compounds, is shown in Figure 3. Peak E of Figure 2 can be seen to be the only feature in common in the two voltammograms (in addition to a small peak D, reduction of H^+ produced only when the initial anodic scan was carried to the point of background decomposition). In addition, a new oxidation peak H, barely evident in Figure 2, appears. The latter peak is assumed to be the oxidation of the e^2 isomer (see $B_{20}H_{18}^{4-}$ in Figure 1 and Scheme I) of $B_{20}H_{16}L_2^{2-}$, the expected reduction product of peak E. Values of $E_{p/2}$ are given in Table IV.

Preparation of $B_{20}H_{16}L_2^{2-}$ Ions. The a^2 isomers were pre-

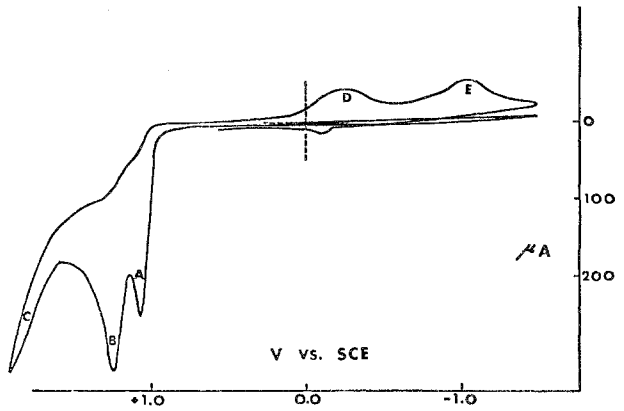

Figure 2. Cyclic voltammogram of $(C_3H_7)_4N[1\text{-}B_{10}H_9S(CH_3)_2]$; scan rate 4 V/min.

Table I. First Anodic Process (Peak A) for B_{10} Species by Stationary-Electrode Voltammetry (Half-Peak Potential *vs.* Sce)

Compd	$E_{p/2}$, V	Compd	$E_{p/2}$, V
$B_{10}H_{10}^{2-}$	+0.40		
$2\text{-}B_{10}H_9I^{2-}$	+0.53	$1\text{-}B_{10}H_9I^{2-}$	+0.53
$2\text{-}B_{10}H_9NH_3^-$	+0.78	$1\text{-}B_{10}H_9NH_3^-$	+0.75
$2\text{-}B_{10}H_9N(CH_3)_3^-$	+0.90	$1\text{-}B_{10}H_9N(CH_3)_3^-$	+0.88
$2\text{-}B_{10}H_9S(CH_3)_2^-$	+0.92	$1\text{-}B_{10}H_9S(CH_3)_2^-$	+0.92

Table II. Methyl Group ^1H Nmr Absorptions of $B_{20}H_{17}L_2^-$ Ions

L	τ,[a] ppm	Rel area	L	τ,[a] ppm	Rel area
$1\text{-}N(CH_3)_3$	6.52	3	$1\text{-}S(CH_3)_2$	7.00	[b]
	6.60	1		7.08	
$2\text{-}N(CH_3)_3$	7.36	3	$2\text{-}S(CH_3)_2$	7.71	3
	7.42	1		7.76	1

[a] $(CH_3)_4Si$ at 10.000 ppm. [b] Relative areas obscured by overlapping pattern of $(C_3H_7)_4N^+$ ion present.

Table III. Nmr Spectral Data for $B_{20}H_{16}L_2$ Compounds

L	^{11}B nmr (32 MHz)[a]	^1H nmr (60 MHz)[b]
$1\text{-}N(CH_3)_3$	Singlet, −10 ppm (2); singlet, +8 ppm (2); complex multiplet, centered at +31 ppm (16)	Singlet, 6.44 ppm
$2\text{-}N(CH_3)_3$	Doublet, −6.4 ppm (2.0) [J_{BH} = 157 Hz]; singlet, +3.9 ppm (2.0); complex multiplet, centered at +33 ppm (16.0)	Singlet, 7.36 ppm
$1\text{-}S(CH_3)_2$	Singlet, −9.4 ppm (1.8); singlet, +15.9 ppm (2.0); complex multiplet, centered at +31 ppm (16.2)	Singlet, 6.88 ppm
$2\text{-}S(CH_3)_2$	Doublet, −9.0 ppm (1.8) [J_{BH} = 156 Hz]; singlet, +3.6 ppm (2.1); complex multiplet, centered at +38 ppm (16.1)	Singlet, 7.63 ppm (1); singlet 7.68 ppm (1)

[a] Chemical shift relative to external $B(OCH_3)_3$; relative areas in parentheses. [b] Chemical shifts given as τ values ($(CH_3)_4Si$ at 10.000 ppm).

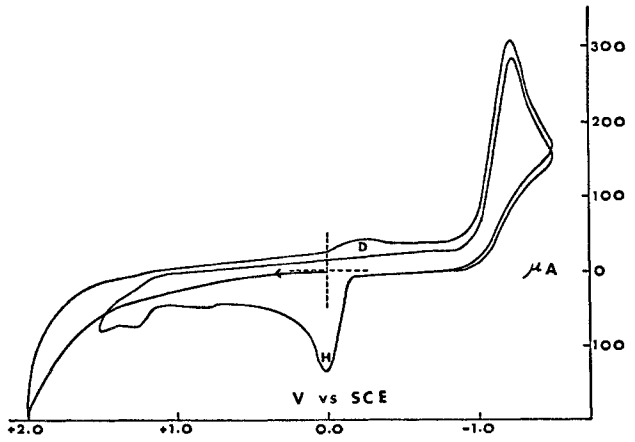

Figure 3. Cyclic voltammogram of apically substituted $B_{20}H_{16}[S(CH_3)_2]_2$; scan rate 4 V/min.

Table IV. $B_{20}H_{16}L_2$ Cathodic Process (Peak E, Figures 2 and 3) and Product Anodic Process (Peak H, Figure 3) by Cyclic Voltammetry (Half-Peak Potential *vs.* Sce)

	$E_{p/2}$, V			$E_{p/2}$, V	
L	Peak E	Peak H	L	Peak E	Peak H
2-$S(CH_3)_2$	−0.89	−0.14	2-$N(CH_3)_3$	−1.28	−0.13
1-$S(CH_3)_2$	−1.08	−0.08	1-$N(CH_3)_3$	−1.27	−0.34

Table V. Nmr Spectral Data for a^2 Isomers of $B_{20}H_{16}L_2^{2-}$ Ions

L	^{11}B nmr (32 MHz)[a]	^1H nmr (60 MHz)[b]
1-$N(CH_3)_3$	Singlet, +3.0 ppm (1.9); singlet, +15.3 ppm (2.2); maximum at +45 ppm, with shoulder at +48 ppm (15.9)	Singlet, +6.53 ppm
2-$N(CH_3)_3$	Singlet, +12.2 ppm (1.8); singlet, +21.6 ppm, with overlapping doublet, +26.2 ppm (4.1) [J_{BH} = 137 Hz]; unsymmetric triplet, centered at +44.6 ppm (14.1)	Singlet, 7.32 ppm
1-$S(CH_3)_2$	Singlet, +5.5 ppm (1.9); singlet, +15.2 ppm (2.0); unsymmetric peak, centered at +43.6 ppm (16.1)	Singlet, 7.08 ppm
2-$S(CH_3)_2$	Singlet, +8.3 ppm (1.8); doublet, +24.2 ppm (2.5) [J_{BH} = 147 Hz]; complex multiplet, centered at +45 ppm (15.7)	Singlet, 7.70 ppm

[a] Chemical shift relative to external $B(OCH_3)_3$; relative areas in parentheses. [b] Chemical shifts given as τ values ($(CH_3)_4Si$ at 10.000 ppm).

pared by reaction of fluorenyllithium with $B_{20}H_{17}L_2^-$ ions. The products were characterized by the nmr spectra of acetonitrile solutions summarized in Table V.

The presumed e^2 isomers with L = 2-$N(CH_3)_3$ and 1-$S(CH_3)_2$ were prepared by reduction of the $B_{20}H_{16}L_2$ compounds with sodium in liquid ammonia and isolated as hydrated potassium salts. The ^1H nmr absorptions of the methyl groups (in aqueous solutions) were at τ values of 8.02 and 8.09 ppm, respectively. No ^{11}B nmr spectra were obtained because of the small amounts and limited solubilities of the salts isolated.

Coupling Reaction Kinetics. Chronopotentiometry with current reversal was used to determine the rate of disappearance of the product of oxidation peak **A**. The data were consistent with second-order kinetics, as expressed in eq 2.

Table VI. Second-Order Rate Constants for Disappearance of One-Electron Transfer Products of $B_{10}H_{10}^{2-}$ Ion and Derivatives at 25°

Starting ion	$10^{-4}k$, M^{-1} sec^{-1}	Starting ion	$10^{-4}k$, M^{-1} sec^{-1}
$B_{10}H_{10}^{2-}$	0.61		
2-$B_{10}H_9I^{2-}$	1.7	1-$B_{10}H_9I^{2-}$	7.1
2-$B_{10}H_9NH_3^-$	6.0	1-$B_{10}H_9NH_3^-$	22
2-$B_{10}H_9N(CH_3)_3^-$	12	1-$B_{10}H_9N(CH_3)_3^-$	34
2-$B_{10}H_9S(CH_3)_2^-$	22	1-$B_{10}H_9S(CH_3)_2^-$	16

The second-order rate constants obtained are given in Table VI.

Discussion

Applicability of Scheme I. The general similarity in appearance of cyclic voltammograms of the $B_{10}H_9L^-$ ions to those of the $B_{10}H_{10}^{2-}$ ion suggests that the overall oxidative processes are similar to those of eq 1-3. These are expressed in eq 4-6. The successful electrolytic preparations of

$$B_{10}H_9L^- \rightleftarrows B_{10}H_9L + e^- \quad (4)$$

$$2B_{10}H_9L \rightarrow B_{20}H_{17}L_2^- + H^+ \quad (5)$$

$$B_{20}H_{17}L_2^- \rightleftarrows B_{20}H_{16}L_2 + H^+ + 2e^- \quad (6)$$

$B_{20}H_{17}L_2^-$ ions and $B_{20}H_{16}L_2$ compounds at appropriate potentials verify the similarity of behavior and the overall validity of eq 4-6. The observed second-order kinetics of disappearance of the product of anodic peak A and the isolation of $B_{20}H_{17}L_2^-$ ions after electrolysis at the potential of peak A confirm eq 4 and 5. Cyclic voltammetry of the isolated $B_{20}H_{17}L_2^-$ ions and the preparation of $B_{20}H_{16}L_2$ compounds by electrolysis of $B_{10}H_9L^-$ ions at the potential of peak B confirm that peak B is described by eq 6.

Structural interpretations of the nmr spectra of the substituted B_{20} species are consistent with the known redox and acid-base chemistry of the unsubstituted B_{20} ions in Scheme I. In the low-field region of the ^{11}B nmr spectra (the region in which apex boron absorptions are expected) of the $B_{20}H_{16}L_2^{2-}$ ions prepared by deprotonation of $B_{20}H_{17}L_2^-$ ions, the presence of two singlets (substituted boron atoms) for ions with apical L groups and one singlet and one doublet (B-H) for ions with equatorial L groups clearly indicate these to be derivatives of the a^2 isomer of $B_{20}H_{18}^{4-}$. The ^1H nmr signals observed for the methyl groups in $B_{10}H_9L^-$, $B_{20}H_{17}L_2^-$, $B_{20}H_{16}L_2$, and the a^2 isomer of $B_{20}H_{16}L_2^{2-}$ (from deprotonation of $B_{20}H_{17}L_2^-$) differ very little in chemical shift for a given L. By contrast, reduction of $B_{20}H_{16}L_2$ compounds produced a significant chemical shift. We conclude that this second isomer is the e^2 isomer of $B_{20}H_{16}L_2^{2-}$ by analogy with the behavior of the unsubstituted species in Scheme I.

The pattern of absorptions in the low-field (apex boron) region of the ^{11}B nmr spectra of the $B_{20}H_{17}L_2^-$ ions is sufficiently complex that it can be said that these ions are highly unsymmetrical, as is the $B_{20}H_{19}^{3-}$ ion itself. The unequal methyl ^1H nmr absorptions of the L groups suggest a mixture of isomers in solution. The linkage between B_{10} units in $B_{20}H_{19}^{3-}$ is not stereochemically rigid on a laboratory scale of minutes, so a mixture of ions isomeric in the stereochemistry of the cage-cage linkage is possible in solution.[2] However, there was no evidence for more than a single isomer of the $B_{20}H_{16}L_2^{2-}$ ions obtained by deprotonation of the $B_{20}H_{17}L_2^-$ ions.

The ^{11}B nmr spectra of the $B_{20}H_{16}L_2$ compounds (Table III) show clearly that the lowest field absorption is due to the apex boron to which the 1-L groups are attached. Steric requirements of the apical $N(CH_3)_3$ and $S(CH_3)_2$ groups

favor the assignment of the lowest field absorption of $B_{20}H_{18}^{2-}$ to the apex borons *most remote* from the cage-cage linkage.

The presence of two absorptions of equal area in the methyl region of the ^1H nmr spectrum of equatorially substituted $B_{20}H_{16}[S(CH_3)_2]_2$ can be explained in two ways. Examination of Figure 1(d) readily reveals the possibility of a variety of geometrical isomers for one equatorial substituent on each B_{10} unit. A fortuitous mixture of two or more of these isomers could give rise to the observed spectrum. A second explanation assumes that a single isomer is present and that the $S(CH_3)_2$ groups are pseudotetrahedral and are at equivalent positions on the B_{10} units. If the position of substitution is *not* at the boron atom in the plane of the four boron atoms involved in the linkage between B_{10} units, the B_{10} units are asymmetric, and the methyl groups on one sulfur atom are not in equivalent environments even if free rotation about the boron-sulfur bond (but not inversion at the sulfur atom) is assumed.[6] A third possibility is that the $S(CH_3)_2$ groups are not at equivalent positions on the two B_{10} units of the $B_{20}H_{16}L_2$ compound. The observation of a single methyl resonance for equatorially substituted $B_{20}H_{16}[N(CH_3)_3]_2$ leads us to favor the second explanation.

Substituent Effects. In Figure 4, log k for reaction 5 is plotted against $E_{p/2}$ for reaction 4. A good linear correlation exists for the equatorial isomers (log $k = 2.46E_{p/2} + 2.85$) but not for the apical isomers. Within a precision of ±0.01 for $E_{p/2}$ and ±10% for k values, $E_{p/2}$ is essentially independent of the position of substitution, but values of k are significantly dependent on the position of substitution.

Substituent constants for I, $N(CH_3)_3^+$, and $S(CH_3)_2^+$ have been reported on the σ_m, σ_p, and σ_p^+ scales. Only the σ_m values come close to linear correlation with log k or $E_{p/2}$. The correlation of log k for equatorial isomers with σ_m is shown in Figure 5. The ρ value for this reaction is 1.56. A very slight apparent curvature in this plot is more evident in the plot of $E_{p/2}$ *vs.* σ_m in Figure 6. The slope of the straight line shown in Figure 6 is 0.76, corresponding to a conventional ρ value of −13. This is not unreasonable by comparison with a ρ value of −20 for the gas-phase electron-impact ionization of substituted benzyl radicals.[7] The good correlations between log k and σ_m and between log k and $E_{p/2}$ for equatorial isomers suggest that a value of σ_m for NH_3^+ (unreported) can be read from the log k *vs.* σ_m plot. A value of 4.78 for log k for the equatorial NH_3 substituent places σ_m for the NH_3^+ group between 0.67 and 0.70, depending on the amount of curvature considered in the log k *vs.* σ_m correlation. It has been determined that the NH_3^+ group is significantly less electron withdrawing than the $N(CH_3)_3^+$ group in aliphatic systems, as measured by σ_I values of 0.60 and 0.90, respectively.[8]

The σ_m scale is generally regarded as being determined primarily by inductive rather than resonance effects, and the σ_p scale by both. The correlation of the rates of reaction 5 for equatorial isomers with the σ_m and not the σ_p scale leads to the conclusion that equatorial substituents exert an essentially inductive rather than resonance effect on this reaction. This is consistent with the effect of equatorial

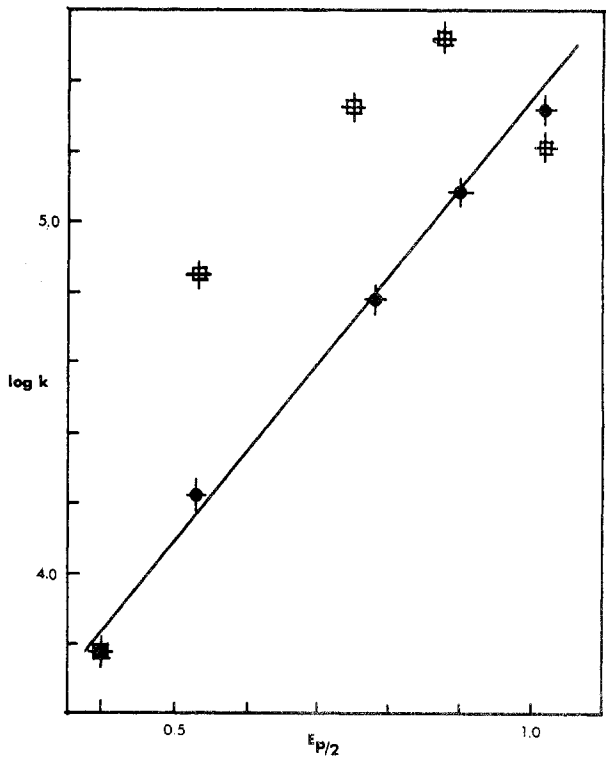

Figure 4. log k for reaction 5 *vs.* $E_{p/2}$ for reaction 4: solid circles, equatorial isomers; open squares, apical isomers.

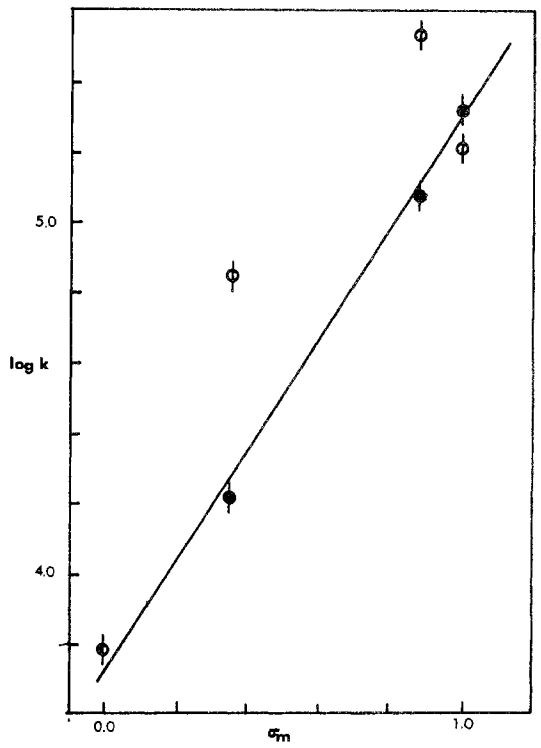

Figure 5. log k for reaction 5 *vs.* σ_m: solid circles, equatorial isomers; open circles, apical isomers.

COOH and NH_2 groups on the uv spectra of diazonium derivatives of the $B_{10}H_{10}^{2-}$ ion.[9]

The data in Table VI show that substituents in an apical position produce a different relative order of k values for reaction 5 than do the same substituents in an equatorial position. However, the $E_{p/2}$ values for reaction 4 given in

(6) L. M. Jackman, "Application of Nuclear Magnetic Resonance in Organic Chemistry," Pergamon Press, New York, N. Y., 1959, pp 99-103.

(7) A. G. Harrison, P. Kebarle, and F. P. Lossing, *J. Amer. Chem. Soc.*, 83, 777 (1961).

(8) R. W. Taft, Jr., cited by P. R. Wells, *Chem. Rev.*, 63, 182 (1963).

(9) W. R. Hertler, W. H. Knoth, and E. L. Muetterties, *Inorg. Chem.*, 4, 288 (1965).

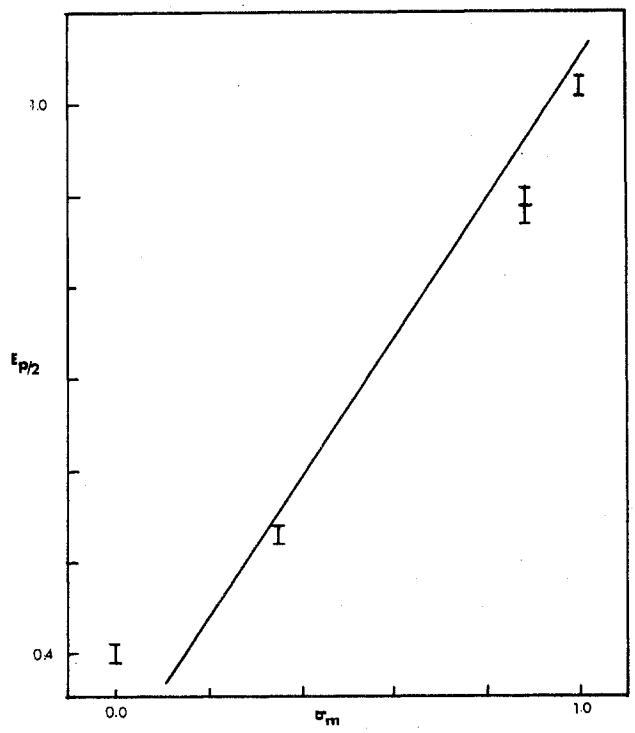

Figure 6. $E_{p/2}$ for reaction 4 *vs.* σ_m.

Table I show the same order regardless of the position of substitution, and this order is the same as that of the k values for the equatorial isomer series which correlate quite well with σ_m values. Thus, we assume that the effects of substituents bonded to boron, including the effects of apical substituents on k values for reaction 5, can be interpreted on the basis of the effects of those same substituents on organic reactions and equilibria.

The first question to be answered is whether the different order of reaction rates for apical and equatorial isomers can be explained by different inductive and resonance contributions to the substituent effects in the two series. There are some 40 different substituent constant scales based on different single reaction series or derived from combinations of reaction series. It has been determined by Swain and Lupton[10] that, of these, no more than two σ sets are significantly independent and that all these sets can be expressed as linear combinations of two independent sets chosen to represent pure field or inductive effects ($\mathcal{F}$), and resonance effects ($\mathcal{R}$). The log k values for apical isomers cannot be expressed as a linear combination of these two parameters for the substituents. Since all of the σ scales based on single reaction series can be expressed as linear combinations of these two parameters, it can be deduced that the log k values will not correlate with any of the single-series σ scales. Furthermore, by examination of the linear coefficients that relate $\mathcal{F}$ and $\mathcal{R}$ to the various σ scales, it can be shown that for all the single reaction series on which σ scales have been based, the order of electron-withdrawing power will be the same: I < $N(CH_3)_3^+$ < $S(CH_3)_2^+$. Thus, the log k values are not even in the same order as substituent effects for a wide variety of organic reaction series involving transition states with developing positive or negative charges and in which resonance effects are dominant or negligible. Although resonance effects may be more important for apical substituents than for equatorial substituents at boron, this cannot account for the log k values unless substituent effects are qualitatively different at boron and carbon and there is a larger difference between the importance of resonance effects at equatorial and apical positions than is encountered in aliphatic and aromatic organic chemistry.

The second question to be answered is whether an explanation for the rate constants in Table VI can be found that is consistent with the order of electron-withdrawing power: I < NH_3^+ < $N(CH_3)_3^+$ < $S(CH_3)_2^+$. The data in Table VI show a definite rate acceleration by electron withdrawal and that this effect is more pronounced for apical than for equatorial substitution. However, in the case of the apical $S(CH_3)_2^+$ substituent, this extreme of electron withdrawal has resulted in a slower rate than observed for the less electron-withdrawing $N(CH_3)_3^+$ substituent. Behavior of this type is indicative of a change in the rate-determining step when the electron withdrawal is sufficiently great.

A change in rate-determining step could arise in two simple ways. The observation that the $B_{20}H_{17}L_2^-$ products are apparently isomeric mixtures suggests that parallel mechanisms leading to isomeric products should be considered. However, this would lead to upward rather than downward curvature in the log k *vs.* electron withdrawal relationship, as the initially slower pathway becomes more rapid than the initially faster pathway. The sequential two-step mechanism described by eq 5a and 5b is more reasonable and is consistent

$$2B_{10}H_9L \rightleftarrows B_{20}H_{18}L_2 \quad (5a)$$

$$B_{20}H_{18}L_2 \rightarrow B_{20}H_{17}L_2^- + H^+ \quad (5b)$$

with the downward curvature of the log k *vs.* electron withdrawal relationship.[11] Since loss of H^+ should be accelerated by electron-withdrawing substituents, we propose that reaction 5b is rate limiting in cases of moderate electron withdrawal, with reaction 5a as a "rapid" prior equilibrium. If reaction 5a is slowed in the forward direction by electron withdrawal, it could become slower than reaction 5b and thus be rate limiting if electron withdrawal is strong enough.

Experimental Section

A. Materials. All chemicals, unless indicated below, were of the highest purity obtainable and were used as received.

Amberlite IR-120 cation-exchange resin obtained from Mallinckrodt Chemical Works was used on the H^+ cycle to convert various anionic compounds from one cation form to another and for equivalent weight determinations.

Acetonitrile for use as a general solvent and for bulk electrolysis was distilled once from CaH_2. For use in electrochemical studies, it was distilled from CaH_2, then from P_4O_{10}, and then again from CaH_2. When distilled in this way, the potential range of 0.1 M solutions of $(C_3H_7)_4NBF_4$ or $(C_2H_5)_4NClO_4$ was +2.1 to −1.8 V *vs.* sce. No electroactive impurities were detected in this range when the solutions were deaerated by bubbling purified N_2 through them for 20 min.

Tetraethylammonium perchlorate and tetrapropylammonium tetrafluoroborate were prepared by the metathetical reaction of the tetraalkylammonium bromide and the sodium salt of the anion in water. The compounds were crystallized twice from water and dried under vacuum at 100°.

B. Instrumentation and Procedures. Infrared spectra were run as KBr pellets or Nujol mulls on a Perkin-Elmer Model 421 spectrophotometer.

Boron-11 nmr spectra were run at 32 MHz on a Varian HA-100 spectrometer in the nonlocked field sweep mode. Spectra were calibrated by the use of audiofrequency side bands. Positive chemical shifts are upfield and have an uncertainty of ±0.5 ppm. Some spectra were run also at 80 MHz by Dr. R. J. Wiersema using a cryogenic magnet nmr spectrometer at UCLA. A Du Pont Model 310 curve resolver was used to analyze some regions of certain spectra. Proton nmr spectra were run on a Varian A-60 or A-60A spectrometer.

(10) C. G. Swain and E. C. Lupton, Jr., *J. Amer. Chem. Soc.*, 90, 4328 (1968).

(11) A quantitative derivation of the curvature resulting for parallel *vs.* sequential transition states is given by R. L. Schowen and K. S. Latham, Jr., *J. Amer. Chem. Soc.*, 89, 4677 (1967).

Cyclic voltammetry was carried out on 10.0 ml of solution containing millimolar concentrations of B_{10} or B_{20} species. Acetonitrile solutions also contained approximately 0.1 *M* $(C_3H_7)_4NBF_4$ or $(C_2H_5)_4NClO_4$ as supporting electrolyte. The solutions were placed in a 50 ml wide-mouth jar and thermostated at 25.0 ± 0.1°. The stationary working electrode was a Beckman Model 39273 platinum-inlay electrode with approximately 0.22-cm^2 surface area. A platinum foil auxiliary electrode was used. The reference electrode was an aqueous saturated calomel electrode. All potentials are reported relative to the sce. Oxygen was removed by bubbling purified N_2, presaturated with the solvent, through these solutions and then blanketing them under N_2 during the experiments.

Current-voltage curves were also obtained using a rotating platinum electrode, constructed by sealing platinum wire in 4-mm o.d. soft-glass tubing, as the working electrode. These data were used to check the reversibility of the electron transfer for the initial oxidation of B_{10} species. This was done by constructing the usual log $[i/(i_l - i)]$ *vs.* E plots.

Bulk electrolyses were carried out on saturated $(C_3H_7)_4NB_{10}H_9L$ acetonitrile solutions. The concentration of these solutions varied with the substituent L but was in the range from 0.05 to 0.1 *M*. The bulk electrolysis H cell was placed in a 150 mm × 75 mm crystallizing dish which was placed on a magnetic stirrer. The anode compartment was flushed with N_2, presaturated with CH_3CN, prior to and during electrolysis. The cathode compartment contained CH_3CN and *ca.* 2 ml of concentrated H_2SO_4. More H_2SO_4 was added to the cathode compartment as the electrolysis proceeded. During the course of the electrolysis the migration of solvated $(C_3H_7)_4N^+$ ions resulted in "pumping" of acetonitrile from the anode to the cathode. As only trace amounts of boron-containing species were found in the cathode compartment and only trace amounts of sulfate were found in the anode compartment, solvated $(C_3H_7)_4N^+$ appeared to be the principal migrating species in solution. This pumping phenomenon was such that generally 15–30 ml of CH_3CN was added to the anode compartment during the course of a one-electron oxidation of 5 mmol of $B_{10}H_9L^-$ to maintain equal volumes of solution in the anode and cathode compartments.

When a large current, *ca.* 150 mA or more, was passed through the electrolysis cell, the glass frit separating anode and cathode compartments would become quite warm. To prevent solvent vaporization in the frit, the frit was cooled by packing ice around it. The crystallizing dish mentioned above served to hold the ice and ice water.

The electrolysis current was supplied by a Kepco Model OPS 40-0.5 power supply. The potential of the working electrode and the power supply output were monitored with a VTVM. The current was monitored by measuring the voltage drop across a 10-ohm wire-wound precision resistor in series with the working electrode. This potential was measured and recorded with a Moseley Model 7101A strip chart recorder. The number of coulombs passed through the electrolysis solution and hence the number of electrons per $B_{10}H_9L^-$ were obtained by manual integration of the trace recorded by the strip chart recorder.

Reverse current chronopotentiometry and cyclic voltammetry experiments were carried out using an instrument built according to a design by Dr. M. D. Hawley.[12] The electrode configuration, cell, and solution concentrations used for the RCC experiments were the same as those described in the voltammetry section above. The platinum-inlay electrode was used exclusively as the working electrode. The rate constants, k, for dimerization following the one-electron oxidation of $B_{10}H_9L^-$ and other B_{10} species were determined from working curves of τ_r/t_f *vs.* log (kt_fC) calculated for an EC dimerization using methods outlined by Feldberg and Auerbach.[13] τ_r was determined by the method of Kuwana as described by Adams.[14]

C. Preparation of Compounds. Literature procedures were used with minor modifications for the preparations of salts of the $B_{10}H_9S(CH_3)_2^-$ ion[15] and $B_{10}H_9NH_3^-$ and $B_{10}H_9N(CH_3)_3^-$ ions.[16,17]

1-$B_{10}H_9I^{2-}$. Two methods were used to convert salts of the $B_{10}H_9IC_5H_5^-$ ion[18] to salts of 1-$B_{10}H_9I^{2-}$.

A solution of 0.04 *M* $CsB_{10}H_9IC_6H_5$ in an acetonitrile–water mixture was electrolyzed at −1.5 to −2.0 V on a mercury pool electrode until the current had decreased to about 10% of its original value. The solution was filtered, after which the addition of saturated aqueous $(CH_3)_4NCl$ caused the precipitation a white solid. Recrystallization produced two fractions, with the major fraction being $Cs(CH_3)_4NB_{10}H_9I$ and the minor fraction being $(CH_3)_4NB_{10}H_9IC_6H_5$.

A solution 6×10^{-3} *M* $CsB_{10}H_9IC_6H_5$ in H_2O or H_2O–CH_3CN was irradiated with a medium-pressure Hg lamp fitted with a Corex filter (290-nm cutoff) for 4–5 hr, during which time O_2 was liberated from the solution and the solution became acidic. After neutralization of the reaction mixture, the addition of $(CH_3)_4NCl$ caused the precipitation of a solid which gave white crystals of $Cs(CH_3)_4NB_{10}H_9I$ when crystallized from H_2O–CH_3CN. The double salt was converted to the more soluble $[(CH_3)_4N]_2B_{10}H_9I$ by ion exchange to the Na^+ salt and the addition of $(CH_3)_4NCl$.

Anal. Calcd for $[(CH_3)_4N]_2B_{10}H_9I$: B, 27.55; equiv wt 199.2. Found: B, 27.11; equiv wt (acid ion exchange) 200.

The infrared spectrum showed absorption maxima (cm^{-1}) at 3020 w, 2515 vs, 2500 vs, 2455 vs, 1490 vs, 1484 s, 1408 w, 1288 vw, 1120 vw, 1099 w, 1020 m, 949 m, 857 vw, 850 vw, 805 vw, 745 vw, 735 vw, 687 vw, 642 vw.

The ^{11}B nmr spectrum of 1-$B_{10}H_9I^{2-}$ consisted of a doublet at +18 ppm [J_{B-H} = 140 Hz] (area 0.8), a singlet at +27.0 ppm (1.0), and an apparent triplet centered at +46.5 ppm (8.2).

2-$B_{10}H_9I^{2-}$. Modification of reported reactions[19,20] gave moderately good yields of 2-$B_{10}H_9I^{2-}$. Gaseous HI was generated over an 8-hr period by the slow addition of 1.0 l. of tetralin, $C_{10}H_{12}$, containing 42.0 g of I_2, to refluxing $C_{10}H_{12}$. Predried N_2 was used to carry the HI into 300 ml of toluene containing 11.17 g (37.2 mol) of 6,9-$[(C_2H_5)_2S]_2B_{10}H_{12}$.[19] Excess HI was driven from the solution by passing N_2 through the solution for an additional 24 hr. Freshly distilled $(C_2H_5)_3N$ (100 ml) was added and the reaction mixture was refluxed under N_2 for 29 hr. The mixture was cooled to room temperature and the toluene solution was decanted from the reaction flask. The amber-colored semisolid was washed with 2-propanol and extracted twice with 150 ml of 1 *M* NaOH. The extract was filtered through Celite filter aid and excess $(C_3H_7)_4NBr$ solution was added to precipitate $[(C_3H_7)_4N]_2B_{10}H_9I$. After two recrystallizations from aqueous ethanol, 12.34 g (20.0 mmol) of powdery white compound was collected.

The infrared spectrum showed absorption maxima (cm^{-1}) at 2975 vs, 2940 s, 2910 m, 2880 s, 2740 vw, 2510 s, 2465 vs, 2430 vs, 1487 s, 1472 vs, 1445 m, 1387 m, 1355 vw, 1330 vw, 1275 vw, 1185 vw, 1173 vw, 1110 w, 1092 w, 1055 m, 1040 m, 1005 m, 990 s, 970 s, 940 vw, 922 vw, 875 vw, 848 w, 800 vw, 790 w, 753 m, 707 vw, 667 vw, 632 w.

The ^{11}B nmr spectrum consisted of a doublet at +18.4 ppm [J_{B-H} = 142 Hz], a doublet at +33.7 ppm [J_{B-H} = 125 Hz], and an apparent unsymmetric singlet with a maximum at +45.0 ppm. These peaks overlapped too much to make integration meaningful. However, the low-field doublet had an approximate relative area of 1.

Anal. Calcd for $[(C_3H_7)_4N]_2B_{10}H_9I$: B, 17.53; equiv wt 308.4. Found: B, 17.40; equiv wt (acid ion exchange) 300.

$B_{20}H_{17}L_2^-$. A 2.82-g (7.70-mmol) sample of $(C_3H_7)_4N[1\text{-}B_{10}H_9S(CH_3)_2]$ was dissolved in 50 ml of triply distilled CH_3CN in the anode compartment of an H cell. The potential of the platinum-daisy electrode was held between +1.00 and +1.05 V for 3.75 hr while 760 C (1.02 electrons per $B_{10}H_9S(CH_3)_2^-$) were passed through the solution. A portion of the anodic solution was added to H_2O and titrated with standardized NaOH. This titration indicated the presence of a 0.5 mol of strong acid per mole of $B_{10}H_9S(CH_3)_2^-$ used. A crystalline precipitate was obtained upon addition of aqueous $(C_3H_7)_4NBr$ to the neutralized aqueous solution and upon addition of an ethanolic solution of $(C_3H_7)_4NBr$ to the remaining anodic solution. These compounds were shown to be identical by a variety of techniques. Recrystallization of the combined precipitates gave 1.719 g (3.23 mmol) of apically substituted $(C_3H_7)_4NB_{20}H_{17}[S(CH_3)_2]_2$.

The infrared spectrum showed absorption maxima (cm^{-1}) at 3018 w, 2975 s, 2940 m, 2910 m, 2740 vw, 2520 s, 2485 vs, 1860 m, 1477 s, 1464 s, 1455 s, 1437 w, 1416 vw, 1381 m, 1346 vw, 1323 m, 1305 vw, 1265 vw, 1255 vw, 1178 vw, 1176 vw, 1153 vw,

(12) Department of Chemistry, Kansas State University, Manhattan, Kans.

(13) S. W. Feldberg and C. Auerbach, *Anal. Chem.*, **36**, 305 (1964); S. W. Feldberg, *Electroanal. Chem.*, **3**, 199 (1969).

(14) R. N. Adams, "Electrochemistry at Solid Electrodes," Marcel Dekker, New York, N. Y., 1969, p 184.

(15) W. H. Knoth, W. R. Hertler, and E. L. Muetterties, *Inorg. Chem.*, **4**, 280 (1965).

(16) W. R. Hertler and M. S. Raasch, *J. Amer. Chem. Soc.*, **86**, 3661 (1964).

(17) M. F. Hawthorne and F. P. Olsen, *J. Amer. Chem. Soc.*, **87**, 2366 (1965).

(18) H. C. Miller, W. R. Hertler, E. L. Muetterties, W. H. Knoth, and N. E. Miller, *Inorg. Chem.*, **4**, 1216 (1965).

(19) S. Hermanek, J. Plesek, B. Stibr, and R. Hanousek, *Collect. Czech. Chem. Commun.*, **33**, 2177 (1968).

(20) B. Stibr, J. Plesek, and S. Hermanek, *Collect. Czech. Chem. Commun.*, **34**, 194 (1969).

1123 vw, 1097 vw, 1035 s, 997 s, 976 s, 963 s, 934 vw, 918 vw, 900 vw, 859 w, 842 w, 810 m, 773 vw, 690 w, 675 vw, 640 m, 623 w, 567 vw, 548 vw, 336 w.

The ^{11}B nmr spectra at both 32 and 80 MHz consisted of unresolved multiplets. Integration of the ^1H nmr spectrum gave a ratio of one $(C_3H_7)_4N^+$ to two $S(CH_3)_2$ groups. *Anal.* Calcd for $(C_3H_7)_4NB_{20}H_{17}[S(CH_3)_2]_2$: B, 39.92. Found: B, 39.83.

By essentially identical techniques, tetrapropylammonium salts of other $B_{20}H_{17}L_2^-$ ions were prepared, with L = equatorial $S(CH_3)_2$, apical $N(CH_3)_3$, and equatorial $N(CH_3)_3$. Potentials used were 0.90, 0.75, and 0.90 V, respectively, and yields were all 80–90%. Products were analyzed by integration of ^1H nmr spectra and by boron analysis. Ir spectra showed terminal BH stretching at about 2500 cm^{-1} and bridge hydrogen at 1850–1860 cm^{-1}.

Apically Substituted $B_{20}H_{16}[S(CH_3)_2]_2$. A 2.90-g (7.931-mmol) sample of $(C_3H_7)_4N[1\text{-}B_{10}H_9S(CH_3)_2]$ was dissolved in 55 ml of triply distilled CH_3CN and electrolyzed in the anode compartment of the H cell at an initial potential at +1.30 V. After 3.33 hr, the electrolysis current had decayed from an initial 240 mA to less than 25 mA. At this point, 1518 C (1.97 electrons per $B_{10}H_9S(CH_3)_2^-$) had passed through the electrolysis solution. The anodic solution was added to 50 ml of ethanol. Upon standing overnight, large, clear, golden-colored, monoclinic crystals formed. After recrystallization from C_2H_5OH–CH_3CN, 0.71 g (2.08 mmol) of apically substituted $B_{20}H_{16}[S(CH_3)_2]_2$ (52.6% based on $B_{10}H_9S(CH_3)_2^-$) was obtained. A 0.3150-g sample of a 50:50 mixture (by ^1H nmr) of $B_{20}H_{16}[S(CH_3)_2]_2$ and $(C_3H_7)_4NB_{20}H_{17}[S(CH_3)_2]_2$ was obtained from the alcoholic filtrate upon addition of aqueous $(C_3H_7)_4NBr$. This indicates an overall yield of 63% of $B_{20}H_{16}[S(CH_3)]_2$.

The infrared spectrum showed absorption maxima (cm^{-1}) at 3015 w, 2925 vw, 2530 vs, 2515 s, 1438 m, 1422 m, 1402 w, 1324 vw, 1110 vw, 1032 w, 990 w, 969 w, 944 w, 900 vw, 875 vw, 848 w, 838 w, 818 w, 798 vw, 747 w, 702 m, 679 w, 583 w, 535 m, 336 w. The 32-MHz ^{11}B nmr spectrum is reported in Table III. At 80 MHz, the high-field multiplet is resolved into low- and high-field doublets each of area 2 and three intermediate doublets each of area 4. *Anal.* Calcd for $B_{20}H_{16}[S(CH_3)_2]_2$: B, 60.89. Found: B, 61.20.

Equatorially Substituted $B_{20}H_{16}[S(CH_3)_2]_2$. A 2.2350-g (6.112-mmol) sample of $(C_3H_7)_4N[2\text{-}B_{10}H_9S(CH_3)_2]$ was dissolved in 60 ml of triply distilled CH_3CN in the anode compartment of the H cell. The potential of the daisy electrode was maintained between +1.00 and +1.20 V for 2.88 hr as 1385 C (2.18 electrons per $B_{10}H_9S(CH_3)_2^-$) was passed through the solution. About halfway through the electrolysis, a precipitate began to form and coat the daisy electrode and inside of the anode compartment. Following electrolysis, the anodic solution and solid were washed into ethanol with CH_2Cl_2. After standing for 48 hr, the precipitate was filtered and recrystallized from C_2H_5OH–CH_3CN. A 0.0940-g sample (2.53 mmol, 82.8% based on $B_{10}H_9S(CH_3)_2^-$) of equatorially substituted $B_{20}H_{16}[S(CH_3)_2]_2$ was collected.

The infrared spectrum showed absorption maxima (cm^{-1}) at 3020 w, 1425 m, 1405 sh, 1325 vw, 1035 w, 990 w, 920 vw, 865 w, 830 w, 735 w, 690 w, 580 w, 550 w. Nmr data are reported in Table III. *Anal.* Calcd for $B_{20}H_{16}[S(CH_3)_2]_2$: B, 60.89. Found: B, 60.45.

Apically Substituted $B_{20}H_{16}[N(CH_3)_3]_2$. A 2.8168-g (7.769-mmol) sample of $(C_3H_7)_4N[1\text{-}B_{10}H_9N(CH_3)_3]$ was dissolved in 60 ml of triply distilled CH_3CN in the anode compartment of the H cell. The potential of the daisy electrode was maintained between +1.00 and +1.20 V for 4.0 hr while 1616 C (2.16 electrons per $B_{10}H_9N(CH_3)_3^-$) was passed through the solution. During the electrolysis, the anode compartment became coated with a precipitate which was washed into ethanol with CH_2Cl_2 following the electrolysis. After the CH_2Cl_2 and CH_3CN had evaporated, the precipitate was filtered and recrystallized from C_2H_5OH–CH_3CN. The yield was 0.9179 g (2.62 mmol, 67.5% based on $B_{10}H_9N(CH_3)_3^-$) of apically substituted $B_{20}H_{16}[N(CH_3)_2]_2$.

The infrared spectrum showed a strong absorption at 2545 cm^{-1}. Nmr data are given in Table III. *Anal.* Calcd for $B_{20}H_{16}[N(CH_3)_3]_2$: B, 61.94. Found: B, 61.25.

Equatorially Substituted $B_{20}H_{16}[N(CH_3)_3]_2$. A 3.1769-g (8.761-mmol) sample of $(C_3H_7)_4N[2\text{-}B_{10}H_9N(CH_3)_3]$ was dissolved in 70 ml of triply distilled CH_3CN in the anode compartment of the H cell. The potential of the daisy electrode was held below +1.25 V for 3.82 hr while 1714 C (2.02 electrons per $B_{10}H_9N(CH_3)_3^-$) was passed through the solution. The anodic solution and precipitate were washed into C_2H_5OH. Following recrystallization from C_2H_5OH–CH_3CN, 1.025 g (2.92 mmol, 66.6% yield based on $B_{10}H_9N(CH_3)_3^-$) of equatorially substituted $B_{20}H_{16}[N(CH_3)_3]_2$ was collected.

The infrared spectrum showed absorption maxima (cm^{-1}) at 3010 vw, 2950 vw, 2540 vs, 1475 s, 1450 s, 1400 m, 1110 vw, 1045 vw, 975 sh, 960 w, 875 m, 845 w, 740 m, 685 m, 580 w, 550 w. Nmr data are given in Table III. In the 80-MHz ^{11}B nmr spectrum, the high-field multiplet consisted of a singlet at 18.3 ppm (area 2), a doublet at 27.1 ppm [J_{B-H} = 140 Hz] (area 4), an apparent singlet at 34.6 ppm (area 8), and a doublet at 45.2 ppm [J_{B-H} = 146 Hz] (area 2). *Anal.* Calcd for $B_{20}H_{16}[N(CH_3)_3]_2$: B, 61.94. Found: B, 61.97.

$B_{20}H_{16}L_2^{2-}$. The a^2 isomers were prepared by the addition of excess fluorenyllithium dissolved in 1,2-dimethoxyethane to milligram quantities of $(C_3H_7)_4NB_{20}H_{17}L_2$. The resulting solutions were evaporated to dryness, and the solids were dissolved in CD_3CN for nmr spectroscopy reported in Table V.

Apically substituted $B_{20}H_{16}[S(CH_3)_2]_2$ and equatorially substituted $B_{20}H_{16}[N(CH_3)_3]_2$ were reduced with sodium in liquid ammonia, and the products were isolated as potassium salts.[2] *Anal.* Calcd for $K_2B_{20}H_{16}[S(CH_3)_2]_2 \cdot 2H_2O$: B, 45.91. Found: B, 44.74. Calcd for $K_2B_{20}H_{16}[N(CH_3)_3]_2 \cdot 2H_2O$: B, 46.51. Found: B, 46.52.

Acknowledgments. We are grateful to Dr. Richard J. Wiersema for the 80-MHz ^{11}B spectra and to Professor Richard L. Schowen for many helpful discussions of substituent effects.

Registry No. $B_{10}H_{10}^{2-}$, 12356-12-6; $[(C_3H_7)_4N]_2(2\text{-}B_{10}H_9I)$, 39436-21-0; $2\text{-}B_{10}H_9NH_3^-$, 39436-09-4; $2\text{-}B_{10}H_9N(CH_3)_3^-$, 39436-15-2; $2\text{-}B_{10}H_9S(CH_3)_2^-$, 39436-12-9; $[(CH_3)_4N]_2(1\text{-}B_{10}H_9I)$, 39436-16-3; $1\text{-}B_{10}H_9NH_3^-$, 39436-08-3; $1\text{-}B_{10}H_9N(CH_3)_3^-$, 39436-14-1; $1\text{-}B_{10}H_9S(CH_3)_2^-$, 39436-11-8; $[(C_3H_7)_4N]\{B_{20}H_{17}[N(CH_3)_3]_2\}$, 39436-23-2; $[(C_3H_7)_4N]\{B_{20}H_{17}[S(CH_3)_2]_2\}$, 39436-22-1; $B_{20}H_{16}[N(CH_3)_3]_2$, 39436-13-0; $B_{20}H_{16}[S(CH_3)_2]_2$, 39436-10-7; $1\text{-}B_{20}H_{16}[N(CH_3)_3]_2^{2-}$, 39436-20-9; $2\text{-}B_{20}H_{16}[N(CH_3)_3]_2^{2-}$, 39436-19-6; $1\text{-}B_{20}H_{16}[S(CH_3)_2]_2^{2-}$, 39436-18-5; $2\text{-}B_{20}H_{16}[S(CH_3)_2]_2^{2-}$, 39436-17-4.